

Evidence for $B \rightarrow K\eta/\gamma$ decays at Belle

R. Wedd,²¹ I. Adachi,⁸ H. Aihara,⁴¹ K. Arinstein,^{1,31} V. Aulchenko,^{1,31} A. M. Bakich,³⁸ V. Balagura,¹² E. Barberio,²¹ A. Bay,¹⁸ K. Belous,¹¹ V. Bhardwaj,³³ M. Bischofberger,²³ A. Bondar,^{1,31} A. Bozek,²⁷ M. Bračko,^{20,13} T. E. Browder,⁷ Y. Chao,²⁶ A. Chen,²⁴ B. G. Cheon,⁶ I.-S. Cho,⁴⁵ Y. Choi,³⁷ J. Dalseno,⁸ M. Dash,⁴⁴ A. Drutskoy,³ S. Eidelman,^{1,31} D. Epifanov,^{1,31} N. Gabyshev,^{1,31} P. Goldenzweig,³ H. Ha,¹⁶ Y. Horii,⁴⁰ Y. Hoshi,³⁹ W.-S. Hou,²⁶ H. J. Hyun,¹⁷ T. Iijima,²² K. Inami,²² A. Ishikawa,³⁴ R. Itoh,⁸ M. Iwasaki,⁴¹ D. H. Kah,¹⁷ N. Katayama,⁸ H. Kawai,² T. Kawasaki,²⁹ H. O. Kim,¹⁷ J. H. Kim,³⁷ Y. I. Kim,¹⁷ Y. J. Kim,⁵ K. Kinoshita,³ B. R. Ko,¹⁶ P. Križan,^{19,13} P. Krokovny,⁸ T. Kuhr,¹⁵ R. Kumar,³³ A. Kuzmin,^{1,31} Y.-J. Kwon,⁴⁵ S.-H. Kyeong,⁴⁵ M. J. Lee,³⁶ S.-H. Lee,¹⁶ T. Lesiak,^{27,4} J. Li,⁷ A. Limosani,²¹ C. Liu,³⁵ D. Liventsev,¹² R. Louvot,¹⁸ A. Matyja,²⁷ S. McOnie,³⁸ H. Miyata,²⁹ R. Mizuk,¹² T. Mori,²² Y. Nagasaka,⁹ M. Nakao,⁸ H. Nakazawa,²⁴ Z. Natkaniec,²⁷ S. Nishida,⁸ O. Nitoh,⁴³ T. Ohshima,²² S. Okuno,¹⁴ H. Ozaki,⁸ P. Pakhlov,¹² G. Pakhlova,¹² C. W. Park,³⁷ H. K. Park,¹⁷ K. S. Park,³⁷ R. Pestotnik,¹³ L. E. Piilonen,⁴⁴ A. Poluektov,^{1,31} H. Sahoo,⁷ Y. Sakai,⁸ O. Schneider,¹⁸ J. Schümann,⁸ K. Senyo,²² M. E. Sevier,²¹ M. Shapkin,¹¹ V. Shebalin,^{1,31} J.-G. Shiu,²⁶ B. Shwartz,^{1,31} J. B. Singh,³³ A. Sokolov,¹¹ S. Stanič,³⁰ M. Starič,¹³ K. Sumisawa,⁸ T. Sumiyoshi,⁴² S. Suzuki,³⁴ G. N. Taylor,²¹ Y. Teramoto,³² K. Trabelsi,⁸ S. Uehara,⁸ Y. Unno,⁶ S. Uno,⁸ P. Urquijo,²¹ Y. Usov,^{1,31} G. Varner,⁷ K. E. Varvell,³⁸ K. Vervink,¹⁸ A. Vinokurova,^{1,31} C. H. Wang,²⁵ M.-Z. Wang,²⁶ P. Wang,¹⁰ Y. Watanabe,¹⁴ J. Wicht,⁸ E. Won,¹⁶ B. D. Yabsley,³⁸ H. Yamamoto,⁴⁰ Y. Yamashita,²⁸ Z. P. Zhang,³⁵ V. Zhilich,^{1,31} V. Zhulanov,^{1,31} T. Zivko,¹³ A. Zupanc,¹³ and O. Zyukova^{1,31}

(Belle Collaboration)

¹*Budker Institute of Nuclear Physics, Novosibirsk, Russia*²*Chiba University, Chiba, Japan*³*University of Cincinnati, Cincinnati, Ohio 45221, USA*⁴*T. Kościuszko Cracow University of Technology, Krakow, Poland*⁵*The Graduate University for Advanced Studies, Hayama, Japan*⁶*Hanyang University, Seoul, South Korea*⁷*University of Hawaii, Honolulu, Hawaii 96822, USA*⁸*High Energy Accelerator Research Organization (KEK), Tsukuba, Japan*⁹*Hiroshima Institute of Technology, Hiroshima, Japan*¹⁰*Institute of High Energy Physics, Chinese Academy of Sciences, Beijing, People's Republic of China*¹¹*Institute of High Energy Physics, Protvino, Russia*¹²*Institute for Theoretical and Experimental Physics, Moscow, Russia*¹³*J. Stefan Institute, Ljubljana, Slovenia*¹⁴*Kanagawa University, Yokohama, Japan*¹⁵*Institut für Experimentelle Kernphysik, Universität Karlsruhe, Karlsruhe, Germany*¹⁶*Korea University, Seoul, South Korea*¹⁷*Kyungpook National University, Taegu, South Korea*¹⁸*École Polytechnique Fédérale de Lausanne (EPFL), Lausanne, Switzerland*¹⁹*Faculty of Mathematics and Physics, University of Ljubljana, Ljubljana, Slovenia*²⁰*University of Maribor, Maribor, Slovenia*²¹*University of Melbourne, School of Physics, Victoria 3010, Australia*²²*Nagoya University, Nagoya, Japan*²³*Nara Women's University, Nara, Japan*²⁴*National Central University, Chung-li, Taiwan, People's Republic of China*²⁵*National United University, Miao Li, Taiwan, People's Republic of China*²⁶*Department of Physics, National Taiwan University, Taipei, Taiwan, People's Republic of China*²⁷*H. Niewodniczanski Institute of Nuclear Physics, Krakow, Poland*²⁸*Nippon Dental University, Niigata*²⁹*Niigata University, Niigata, Japan*³⁰*University of Nova Gorica, Nova Gorica, Slovenia*³¹*Novosibirsk State University, Novosibirsk, Russia*³²*Osaka City University, Osaka, Japan*³³*Panjab University, Chandigarh, India*³⁴*Saga University, Saga, Japan*³⁵*University of Science and Technology of China, Hefei, People's Republic of China*³⁶*Seoul National University, Seoul, South Korea*

³⁷*Sungkyunkwan University, Suwon, South Korea*³⁸*University of Sydney, Sydney, New South Wales, Australia*³⁹*Tohoku Gakuin University, Tagajo, Japan*⁴⁰*Tohoku University, Sendai, Japan*⁴¹*Department of Physics, University of Tokyo, Tokyo, Japan*⁴²*Tokyo Metropolitan University, Tokyo, Japan*⁴³*Tokyo University of Agriculture and Technology, Tokyo, Japan*⁴⁴*IPNAS, Virginia Polytechnic Institute and State University, Blacksburg, Virginia 24061, USA*⁴⁵*Yonsei University, Seoul, South Korea*

(Received 6 August 2009; published 28 June 2010)

We present the results of a search for the radiative decay $B \rightarrow K\eta'\gamma$ and find evidence for $B^+ \rightarrow K^+ \eta'\gamma$ decays at the 3.3 standard deviation level with a partial branching fraction of $(3.6 \pm 1.2 \pm 0.4) \times 10^{-6}$, where the first error is statistical and the second systematic. This measurement is restricted to the region of combined $K\eta'$ invariant mass less than $3.4 \text{ GeV}/c^2$. A 90% confidence level upper limit of 6.4×10^{-6} is obtained for the partial branching fraction of the decay $B^0 \rightarrow K^0 \eta'\gamma$ in the same $K\eta'$ invariant mass region. These results are obtained from a 605 fb^{-1} data sample containing $657 \times 10^6 B\bar{B}$ pairs collected at the $\Upsilon(4S)$ resonance with the Belle detector at the KEKB asymmetric-energy e^+e^- collider.

DOI: 10.1103/PhysRevD.81.111104

PACS numbers: 13.25.Hw, 14.40.-n, 14.40.Df, 14.40.Nd

Radiative B meson decays proceed primarily through the flavor changing neutral current quark-level process $b \rightarrow s\gamma$. Flavor changing neutral current processes are forbidden at tree level within the standard model (SM), and hence $b \rightarrow s\gamma$ must proceed via radiative loop diagrams. As loop processes may include unknown heavy particles mediating the loop, any disparity between experimental measurement and SM prediction could be evidence of such new particles.

The world average experimental branching fraction (BF) for the meson-level process $B \rightarrow X_s \gamma$ ($(3.55 \pm 0.26) \times 10^{-4}$ [1]) and the theoretical SM predictions ($(3.15 \pm 0.23) \times 10^{-4}$ [2]) are consistent. Measurements of individual exclusive $B \rightarrow X_s \gamma$ modes, such as $B \rightarrow K\eta'\gamma$, provide consistency checks on the agreement between theory and experiment, and improve our understanding of the hadronization process in $B \rightarrow X_s \gamma$ and $B \rightarrow X_s \ell^+ \ell^-$.

The analysis of the decay mode $B \rightarrow K\eta'\gamma$ uses 605 fb^{-1} of data collected at the $\Upsilon(4S)$ resonance with the Belle detector. This decay was previously studied by *BABAR*, which set upper limits (ULs) of $\mathcal{B}(B^+ \rightarrow K^+ \eta'\gamma) < 4.2 \times 10^{-6}$ and $\mathcal{B}(B^0 \rightarrow K^0 \eta'\gamma) < 6.6 \times 10^{-6}$ at 90% confidence level (C.L.) from an analysis of 211 fb^{-1} of data [3,4].

When the modes $B \rightarrow K\eta$ and $B \rightarrow K\eta'$ were experimentally measured [5,6], a suppression of the former with respect to the latter was evident. Although this had been predicted as a result of the destructive interference between two penguin amplitudes [7], it did not agree with the accepted theory of the time and was considered a possible sign of new physics. The ability of QCD factorization techniques to correctly predict this BF hierarchy has since been demonstrated, though the errors are large [8]. A similar comparison of the observed $B \rightarrow K\eta\gamma$ mode [9] and the previous upper limits for $B \rightarrow K\eta'\gamma$ displays an opposite BF hierarchy. The analogous QCD calculation has

not yet been performed for these decay modes. Measurement of $B \rightarrow K\eta'\gamma$ will provide the necessary experimental benchmark with which to test such a calculation. In addition, a time-dependent charge-parity (CP) asymmetry analysis will be possible for the decay $B^0 \rightarrow K_S^0 \eta'\gamma$ if sufficient statistics are measured. Such mixing-induced CP asymmetries are suppressed within the SM, however, some beyond-SM theories involving right-handed currents allow them to have large values, even when the $B^0 \rightarrow K_S^0 \eta'\gamma$ BF agrees with SM predictions [10].

The Belle detector is designed to identify and measure particles from $\Upsilon(4S) \rightarrow B\bar{B}$ decays [11]. It is located at the interaction point (IP) of the KEKB accelerator in Tsukuba, Japan, which collides electrons and positrons at energies of 8 GeV and 3.5 GeV, respectively [12]. Charged particle tracking and momentum measurements are provided by a silicon vertex detector and a helium/ethane central drift chamber (CDC). Particle identification (PID) is performed using the CDC in conjunction with an array of aerogel Cherenkov counters and time-of-flight scintillators. Electrons and photons are identified and their energy measured by an electromagnetic calorimeter (ECL) of thallium-doped cesium iodide crystals. These detectors are within a 1.5 T magnetic field provided by a superconducting solenoid. A layered iron and resistive plate counter detector outside the solenoid detects K_L^0 mesons and provides discrimination between μ leptons and charged hadrons.

The primary signature of a $B \rightarrow K\eta'\gamma$ event is a high energy photon, which we reconstruct as an isolated shower in the ECL barrel ($32^\circ < \theta < 129^\circ$), with shape consistent with a single photon hypothesis and no associated charged track. Only photons within the range $1.8 \text{ GeV} < E_\gamma^* < 3.4 \text{ GeV}$ are considered, where the asterisk denotes the

$e^+ e^-$ center-of-mass (CM) frame. All other photons in the analysis are required to have energies greater than 50 MeV. Contamination from η and π^0 mesons decaying to $\gamma\gamma$ is reduced using a likelihood technique based on probability density functions (PDFs) extracted from a sample of Monte Carlo (MC) simulated data. The MC sample is designed to mimic normal detector conditions [13]. The likelihood algorithm combines the candidate signal photon with each other photon in the event in turn and assigns a probability for the combination originating from either a π^0 or η decay, based on the combined invariant mass and the energy of the secondary photon. Candidates with any single combination yielding a probability of greater than 0.25 are vetoed. These vetoes remove over 45% of $e^+ e^- \rightarrow q\bar{q}$ MC while passing 91% of signal MC. If more than one signal photon candidate in an event passes these selection criteria, the most energetic is taken as the primary photon from the B meson decay.

Candidate η' mesons are reconstructed in the $\eta' \rightarrow \eta\pi^+\pi^-$ and $\eta' \rightarrow \rho^0\gamma$ modes. Here, η mesons are reconstructed as $\eta \rightarrow \gamma\gamma$ and $\eta \rightarrow \pi^+\pi^-\pi^0$, ρ^0 and K_S^0 mesons are reconstructed as $\pi^+\pi^-$ pairs, and π^0 mesons as $\gamma\gamma$ pairs. Charged kaons and pions are separated using a PID selection with an efficiency for kaons (pions) of 85% (98%) and a misidentification probability of 12% (14%). PID information combined with a measurement of the energy deposited in the ECL is used to reduce electron contamination.

The mass windows chosen to select candidates for each B meson daughter particle are symmetric and of width $\pm 3\sigma$, except where the attributes of the individual particle decays dictate other choices. The exact selection criteria are described below. K_S^0 candidates must pass a set of momentum-dependent selection criteria based on proximity to IP, flight length, and the angle between the momentum vector and reconstructed vertex vector. In this case, the momentum vector is defined as the direction of momentum of the combined pions, and the vertex vector is defined as connecting the IP to the reconstructed π^+ and π^- vertex. Candidates with invariant masses 10 MeV/ c^2 or more from the nominal K_S^0 mass of 497.7 MeV/ c^2 [14] are rejected, where the allowed range is equivalent to a window of 4 standard deviations (σ) of the natural mass width convolved with detector mass resolution. The wider mass selection window for the K_S^0 was chosen to maximize the possibility of a significant result in the neutral modes. Neutral pion candidates must have momenta greater than 100 MeV/ c and $\gamma\gamma$ combined invariant masses in the range $119 \text{ MeV}/c^2 (2.5\sigma) < M_{\gamma\gamma} < 152 \text{ MeV}/c^2 (3\sigma)$. This asymmetric mass window was chosen to reduce the large background of low energy photons due to interactions of the beam with the beam pipe wall and residual gas molecules.

Photons of energy greater than 100 MeV are used to reconstruct $\eta \rightarrow \gamma\gamma$ candidates, which must have

invariant masses in the range $490 \text{ MeV}/c^2 (4\sigma) < M_{\gamma\gamma} < 590 \text{ MeV}/c^2 (3\sigma)$. The asymmetric mass window accepts a greater extent of the low energy tail characteristic of radiative decay invariant mass spectra. The inclusion of low energy background photons is not as significant for $\eta \rightarrow \gamma\gamma$ as for $\pi^0 \rightarrow \gamma\gamma$, as the number of background photons drops significantly as energy increases. Candidates are also required to satisfy the helicity angle requirement $|\cos\theta_{\text{hel}}| < 0.9$, where θ_{hel} is the angle between the momentum vectors of the η' and one of the decay γ 's in the η rest frame. Candidates for the decay $\eta \rightarrow \pi^+\pi^-\pi^0$ must have invariant masses in the range $536 \text{ MeV}/c^2 (3\sigma) < M_{\pi^+\pi^-\pi^0} < 560 \text{ MeV}/c^2 (3\sigma)$. The momenta of all η candidates are then corrected using mass-constrained vertex fits. Candidate ρ^0 mesons must have invariant masses within the range $550 \text{ MeV}/c^2 (3\sigma) < M_{\pi^+\pi^-} < 950 \text{ MeV}/c^2 (3\sigma)$ and pass a helicity requirement similar to the η . A fit constraining the pion vectors to a common vertex must converge with a χ^2/ndof less than 100.

Candidates for the decay $\eta' \rightarrow \rho^0\gamma$ must have invariant masses in the range $945 \text{ MeV}/c^2 (2\sigma) < M_{\rho^0\gamma} < 970 \text{ MeV}/c^2 (2\sigma)$, and the photon must have energy greater than 200 MeV. Candidates for the decay $\eta' \rightarrow \eta\pi^+\pi^-$ must have invariant masses within the range $950 \text{ MeV}/c^2 (2\sigma) < M_{\eta\pi^+\pi^-} < 965 \text{ MeV}/c^2 (2\sigma)$. Function fitting experiments on MC samples, similar to those used to estimate fitting bias (described below), found tighter mass selection windows for the η' offered the greatest chance of a significant measurement. Both types of candidates are also required to have momenta greater than 1.0 GeV/ c as measured in the CM frame. A mass-constrained vertex fit is then applied to all η' candidates. The resulting corrected momenta are used to calculate the kinematic variables M_{bc} and ΔE , described in the next paragraph; only uncorrected momenta are used in selecting η' candidates.

The invariant mass of the $K\eta'$ system ($M_{K\eta'}$) is required to be less than 3.4 GeV/ c^2 , which retains almost all events that pass the lower photon energy requirement. Two kinematic variables are defined: $M_{\text{bc}} \equiv (1/c^2) \times \sqrt{E_{\text{beam}}^2 - (\vec{p}_{K\eta'}^* + \vec{p}_\gamma^*)^2 c^2}$ and $\Delta E \equiv E_B^* - E_{\text{beam}}$, where E_B^* is the energy of the candidate B meson in the CM frame, E_{beam} is half the total CM energy ($\sqrt{s}/2$), and $\vec{p}_{K\eta'}^*$ and \vec{p}_γ^* are the CM frame momenta of the $K\eta'$ combination and the signal photon, respectively. In the calculation of M_{bc} , the momentum of the signal photon is rescaled to be $p_\gamma^* = (1/c)(E_{\text{beam}} - E_{K\eta'}^*)$. Candidate B mesons must satisfy $|\Delta E| < 0.3 \text{ GeV}$ and $5.20 \text{ GeV}/c^2 < M_{\text{bc}} < 5.29 \text{ GeV}/c^2$, and the signal region is defined as $-0.1 \text{ GeV} < \Delta E < 0.07 \text{ GeV}$ and $5.27 \text{ GeV}/c^2 < M_{\text{bc}} < 5.29 \text{ GeV}/c^2$. The signal region is used for data projection purposes.

Backgrounds are estimated using large MC samples [15]. The dominant background is from $e^+ e^- \rightarrow q\bar{q}$ ($q = u, d, s, c$) continuum processes. To reduce this we form a

Fisher discriminant [16] from 16 modified Fox-Wolfram moments [17] and the scalar sum of the event transverse momenta. Fox-Wolfram moments provide a quantification of the sphericity of a group of vectors, helping to distinguish between isotropic $e^+e^- \rightarrow B\bar{B}$ events and jetlike continuum events. The Fisher discriminant is trained on signal MC and sideband data to maximize discrimination between the two. The data sideband regions are defined as $M_{bc} < 5.26 \text{ GeV}/c^2$ and either $\Delta E < -0.2 \text{ GeV}$ or $\Delta E > 0.1 \text{ GeV}$. A likelihood ratio (LR) is formed from the optimized Fisher discriminant, the cosine of the angle between the B meson flight direction and the positron beam axis, and the distance along the positron beam axis between the two B meson vertices, which are reconstructed from the silicon vertex detector and CDC response to charged particles. The acceptance regions of the LR distributions are chosen by maximizing the figure of merit defined as $\mathcal{N}_S/(\sqrt{\mathcal{N}_S + \mathcal{N}_{SB}})$, where \mathcal{N}_S is the number of $B \rightarrow K\eta'\gamma$ MC events that lie above a certain LR value and \mathcal{N}_{SB} is the corresponding number of sideband data events lying above the same value. Both samples are scaled to the number of events expected in 605 fb^{-1} of data, using the central values of the BFs found in the *BABAR* $B \rightarrow K\eta'\gamma$ analysis [3] as hypothetical signal BFs, and the ratio of events in the full fitting region to the sideband region in $q\bar{q}$ MC as the data sideband scaling factor. A previous analysis at Belle [18] found that use of flavor-tagging algorithms can provide greater continuum discrimination. The algorithm calculates the likelihood that an event included one of several highly recognizable B meson decays; this is referred to as the tag “quality.” Events which have a high flavor-tagging quality are less likely to have originated from continuum processes. This information is utilized by optimizing of the figure of merit in seven bins of flavor-tagging quality, as calculated by the Belle B -flavor-tagging algorithm [19]. We accept events with LR values above the point of maximum figure of merit in each bin. The LR requirements are 38% efficient for signal MC and remove 98% of background.

Of the K^+ mesons selected in $b \rightarrow c$ background events, over half originate from the decay of D^0 mesons. To suppress $D^0 \rightarrow K^-\pi^+$ decays, charged kaon candidates are combined with all charged pions in the event in turn. Any candidate which forms a combined invariant mass within the range $1.84 \text{ GeV}/c^2 < M_{K^-\pi^+} < 1.89 \text{ GeV}/c^2$ is removed from consideration. This removes 14% of charged $b \rightarrow c$ events and retains 97.5% of charged signal events. $B \rightarrow J/\psi K \rightarrow (\eta'\gamma)K$ events are suppressed by vetoing candidates with a combined $\eta'\gamma$ invariant mass within $\pm 25 \text{ MeV}/c^2$ of the nominal J/ψ mass [14]. This decay has an averaged BF of $\sim 1 \times 10^{-6}$ [14], which is of the same order as that expected for $B \rightarrow K\eta'\gamma$, and has identical final state particles. In a MC sample equivalent to more than 40 times the available data, no $B \rightarrow J/\psi K$ events pass both selection criteria and veto.

On average, 1.24 candidates per signal MC event pass the selection criteria. A series of discriminating criteria are used to choose the best candidate. These are, in order of implementation, the lowest B vertex χ^2/ndof , the lowest $\rho^0 \rightarrow \pi^+\pi^-$ or $\eta' \rightarrow \eta\pi^+\pi^-$ vertex χ^2/ndof , the reconstruction with η candidate invariant mass closest to the nominal value [14] or the highest E_γ from $\eta' \rightarrow \rho^0\gamma$, and the lowest K_S^0 vertex χ^2/ndof . Candidates that are identical in a criterion cascade to the next criteria until a best candidate is determined. This technique selects the correct candidate in 76% of cases.

Signal yields are extracted using extended unbinned maximum likelihood fits to ΔE and M_{bc} . All reconstructed charged events are combined and a fit performed on the resulting distribution. Similarly, all reconstructed neutral events are combined and a second fit performed on this distribution. The choice of functions and initial parameter values are determined separately for charged and neutral modes from their respective MC distributions. The signal distributions are modeled with Crystal Ball line shapes (CBLS) [20] for M_{bc} , and the sum of a CBLS and a Gaussian function with common means and relative widths for ΔE . The means and widths of the CBLS functions describing the signal distributions in ΔE and M_{bc} are calibrated using large control samples of $B \rightarrow K^*(892)\gamma$ data and MC. The $b \rightarrow c$ background distributions of the charged modes are modeled with ARGUS [21] functions for M_{bc} and second order Chebyshev polynomials for ΔE . These functions did not provide a good fit to the neutral modes $b \rightarrow c$ distribution, and a two-dimensional (2D) Keys PDF [22] was substituted. The Keys PDFs implemented here use Gaussian kernel estimation to provide an unbinned and nonparametric estimate of the probability distribution function from which the fitted data is drawn. The $b \rightarrow u, d, s$ background distributions for both charged and neutral modes are modeled with 2D Keys PDFs. The $e^+e^- \rightarrow q\bar{q}$ distributions are modeled with ARGUS functions for M_{bc} and first order Chebyshev polynomials for ΔE .

The product of the PDFs describing M_{bc} and ΔE for each modeled component is taken as the 2D PDF for that component. The 2D PDFs describing the signal, $e^+e^- \rightarrow q\bar{q}$, $b \rightarrow c$, and $b \rightarrow u, d, s$ distributions are summed to form the total 2D PDFs for charged and neutral modes. These are used to fit the 605 fb^{-1} of accumulated data. The normalizations of the $b \rightarrow c$ and $b \rightarrow u, d, s$ components are fixed to values expected from MC studies; 110(45) events and 12(3) events, respectively, for charged(neutral) modes. The signal and $e^+e^- \rightarrow q\bar{q}$ normalizations and the $e^+e^- \rightarrow q\bar{q}$ PDF parameters are allowed to float, except for the ARGUS endpoint, which is fixed to $5.29 \text{ GeV}/c^2$. Figure 1 shows the results of the $B^+ \rightarrow K^+\eta'\gamma$ and $B^0 \rightarrow K_S^0\eta'\gamma$ fits to data, where the M_{bc} plots show a projection in the ΔE signal region and the ΔE plots show a projection in the M_{bc} signal region.

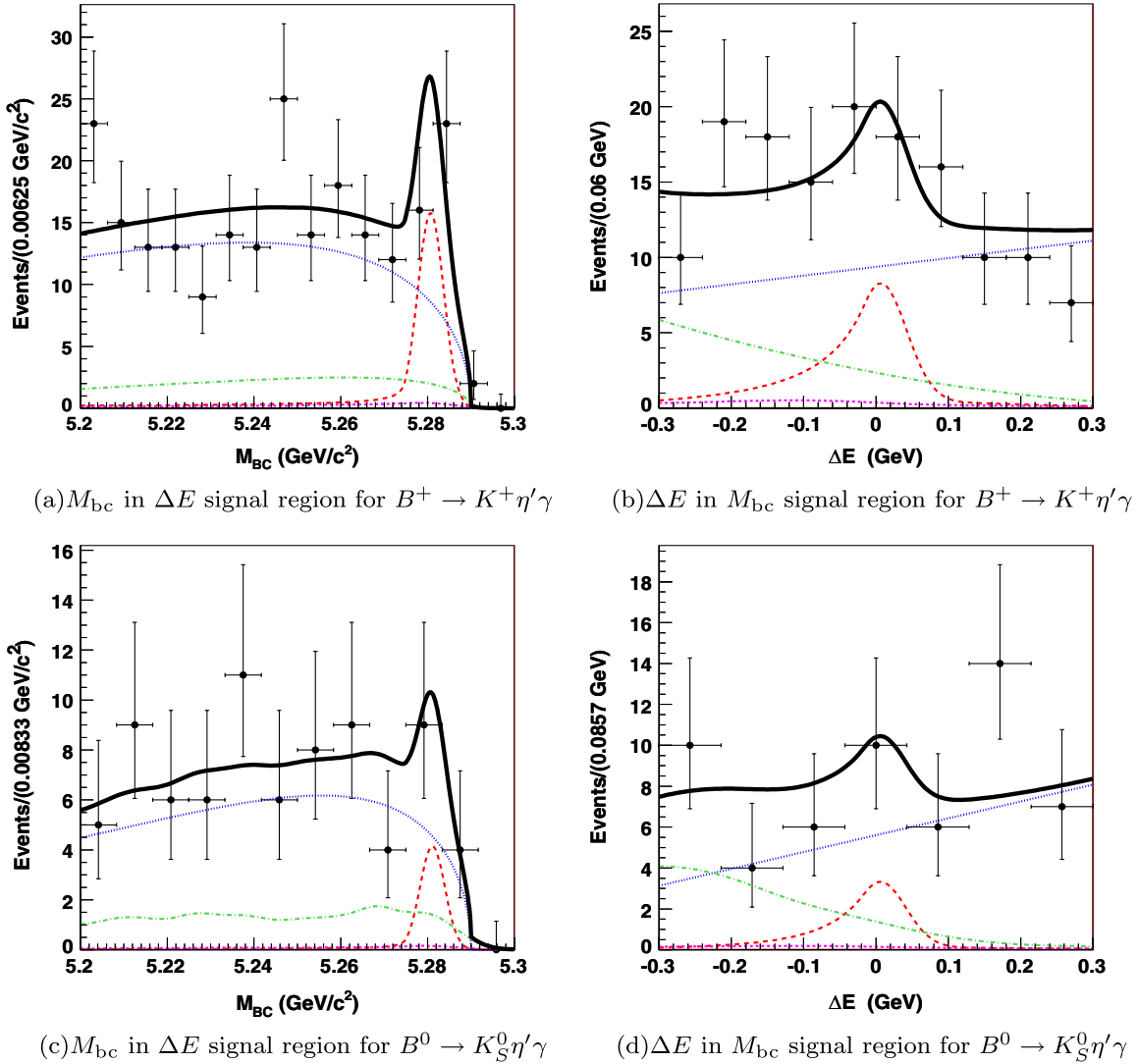


FIG. 1 (color online). Projections to the signal region from the fits to 605 fb^{-1} of data. Each plot is the distribution of one 2D fit variable within the signal region of the second 2D fit variable. In each plot the solid line is the combined background plus signal PDF, the dotted line is the $e^+e^- \rightarrow q\bar{q}$ PDF, the dot-dashed the $b \rightarrow c$ PDF, the long dashed the signal PDF, and the short dashed the $b \rightarrow u, d, s$ PDF.

Table I shows the measured yields and signal significances for the fits to data. We find 33_{-11}^{+12} $B^+ \rightarrow K^+\eta'\gamma$ events for the fit to the charged modes and 5_{-4}^{+5} $B^0 \rightarrow K_S^0\eta'\gamma$ events for the fit to the neutral modes. The fitted $e^+e^- \rightarrow q\bar{q}$ distributions yield 630 ± 28 events for the charged modes and 191 ± 16 events for the neutral modes. The signal significance is defined as $\sqrt{-2 \ln(L_0/L_{\max})}$, where

L_{\max} and L_0 are the values of the likelihood function when the signal yield is floated or fixed to zero, respectively. The systematic errors described below are included in the significances by convolving the likelihood functions with Gaussians of width defined by the magnitude of the errors. The signal significances including systematic errors are

TABLE I. The yields, efficiencies (ϵ), daughter branching fraction products (Π), measured branching fractions (\mathcal{B}), signal significances including systematics (S) and 90% C.L. ULs for the measured decays.

Mode	Yield(events)	ϵ	Π	$\mathcal{B}(10^{-6})$	$S(\sigma)$	UL(10^{-6})
$B^+ \rightarrow K^+\eta'\gamma$	$32.6_{-10.8}^{+11.8}$	0.024	0.571	$3.6 \pm 1.2 \pm 0.4$	3.3	5.6
$B^0 \rightarrow K_S^0\eta'\gamma$	$5.1_{-4.0}^{+5.0}$	0.016	0.197	$2.5_{-1.9-0.5}^{+2.4+0.4}$	1.3	6.4

3.3σ and 1.3σ for the charged modes and neutral modes, respectively.

Any bias in the fitting process is determined using 1000 pseudoexperiments of MC with components of size equal to the yields in the fits to data. The $e^+e^- \rightarrow q\bar{q}$ and $b \rightarrow c$ MC components are generated from the shape of the PDFs, while the signal and $b \rightarrow u, d, s$ components are fully simulated. No significant bias is found in the analysis of these samples.

The signal MC reconstruction efficiencies are calculated as the number of signal events passing the selection criteria divided by the number generated. To calibrate for $M_{K\eta'}$ dependence, scaled sideband $M_{K\eta'}$ data distributions are subtracted from $M_{K\eta'}$ distributions in the full $M_{bc}:\Delta E$ region. The remaining events are unfolded using MC efficiencies as a function of $M_{K\eta'}$. The ratios of events in the background-subtracted distributions over events in the unfolded distributions are taken as the global efficiencies.

The effect of cross feeds, defined as $K_S^0\eta'\gamma$ events being reconstructed as $K^+\eta'\gamma$ and entering the incorrect fit distribution, and *vice versa*, is estimated to bias both the yields and efficiencies reported by +6% (−6%) for charged (neutral) modes from signal MC studies. As this effect is present in both the yields and efficiencies, it has no effect on calculated branching fractions or upper limits. A systematic error of $\pm 6\%$ is assigned to encompass any differences in the level of cross feed between data and MC.

The BFs are calculated from the signal yields, calibrated efficiencies, daughter BF products, and the number of B mesons in the data sample. Equal production of charged and neutral B meson pairs is assumed. We find $\mathcal{B}(B^+ \rightarrow K^+\eta'\gamma) = (3.6 \pm 1.2 \pm 0.4) \times 10^{-6}$ and $\mathcal{B}(B^0 \rightarrow K^0\eta'\gamma) = (2.5_{-1.9-0.5}^{+2.4+0.4}) \times 10^{-6}$, where the first errors are statistical and the second systematic. The 90% C.L. ULs are found to be $\mathcal{B}(B^+ \rightarrow K^+\eta'\gamma) < 5.6 \times 10^{-6}$, and $\mathcal{B}(B^0 \rightarrow K^0\eta'\gamma) < 6.4 \times 10^{-6}$. The ULs are calculated by integrating the likelihood function with systematic errors included in the physically allowed BF region. The UL is then defined as the BF below which 90% of the integrated likelihood lies. The BFs and ULs are measured within the reduced phase-space region $M_{K\eta'} < 3.4 \text{ GeV}/c^2$.

The systematic uncertainties for the charged (neutral) BF include errors on the following processes: photon detection [2.8% (2.8%)]; π^0 reconstruction [0.8% (0.5%)]; K_S^0 reconstruction [0.0% (4.5%)]; η reconstruction [3.4% (3.6%)]; charged track detection [3.8% (5.0%)]; K^+/π^+ differentiation [1.4% (1.5%)]; and the calculated number of $B\bar{B}$ pairs in the data sample [1.4% (1.4%)]. The statistical uncertainty on the MC efficiency after calibration is 1.7% (1.9%). The data/MC LR selection efficiency difference is calculated to be 0.981 ± 0.037 for both fits using a

$B \rightarrow K^*(892)\gamma$ control sample: the central value is applied as a correction to the reconstruction efficiency, and a systematic error of 3.7% is assigned. The vetoes on $M_{\eta'\gamma}$ around the J/ψ invariant mass and on $M_{K^-\pi^+}$ around the D^0 mass are found to affect the reconstruction efficiency by 0.2% (0.4%) and 0.5% (0.0%), respectively. The bias study results have an uncertainty of 1.5% (3.5%). The correction of the signal reconstruction efficiency from the $M_{K\eta'}$ distributions has an uncertainty of 1.2% (1.5%). The effect of cross feed, as previously mentioned, is estimated using signal MC, and yields a 6% (6%) efficiency uncertainty. All fixed parameters in the fit to data are varied by $\pm 1\sigma$, and the $b \rightarrow c$ and $b \rightarrow u, d, s$ fixed normalizations by ± 3 times the square root of the total normalization. The effects of these changes on the measured signal yields were added in quadrature to give uncertainties of (+6.5%, −6.7%) in the $B^+ \rightarrow K^+\eta'\gamma$ BF, and (+11.7%, −16.6%) in the $B^0 \rightarrow K_S^0\eta'\gamma$ BF.

The existing measurements of $B \rightarrow X_s\gamma$ and $B \rightarrow X_s\ell^+\ell^-$ [23–26] rely heavily on the accuracy of the X_s hadronization model performed by the JETSET [27] program. A large sample of inclusive $B \rightarrow X_s\gamma$ MC was generated according to the Kagan-Neubert model [28] with the mass of the b quark set to $4.75 \text{ GeV}/c^2$ (KN475). The X_s system was then hadronized by JETSET. From this sample, the BF of $B^+ \rightarrow K^+\eta'\gamma$ events in the region $M_{K\eta'} < 3.4 \text{ GeV}/c^2$ was calculated as $(1.8 \pm 0.2) \times 10^{-6}$, while we measure $(3.6 \pm 1.2 \pm 0.4) \times 10^{-6}$. In addition, the BF of the decay mode $B \rightarrow K\eta\gamma$ in the MC sample was calculated to be $(8.2 \pm 0.9) \times 10^{-6}$, which can be compared to the measured BF of $(7.9 \pm 0.9) \times 10^{-6}$ [14]. With the current statistics, the BFs for both $B^+ \rightarrow K^+\eta'\gamma$ and $B \rightarrow K\eta\gamma$ are consistent with the KN475 model and the employed tuning of the JETSET hadronization model.

In conclusion, we report the first evidence of the decay $B^+ \rightarrow K^+\eta'\gamma$ with a partial branching fraction of $\mathcal{B}(B^+ \rightarrow K^+\eta'\gamma) = (3.6 \pm 1.2 \pm 0.4) \times 10^{-6}$ and a significance of 3.3σ in the region $M_{K\eta'} < 3.4 \text{ GeV}/c^2$. We also set a 90% confidence level upper limit of $\mathcal{B}(B^0 \rightarrow K^0\eta'\gamma) < 6.4 \times 10^{-6}$ in the same $M_{K\eta'}$ region.

We thank the KEKB group for excellent operation of the accelerator, the KEK cryogenics group for efficient solenoid operations, and the KEK computer group and the NII for valuable computing and SINET3 network support. We acknowledge support from MEXT, JSPS, and Nagoya's TLPRC (Japan); ARC and DIISR (Australia); NSFC (China); DST (India); MOEHRD and KOSEF (Korea); MNiSW (Poland); MES and RFAAE (Russia); ARRS (Slovenia); SNSF (Switzerland); NSC and MOE (Taiwan); and the DOE (USA).

- [1] E. Barberio *et al.*, (Heavy Flavor Averaging Group), <http://arxiv.org/abs/0808.1297>.
- [2] M. Misiak *et al.*, *Phys. Rev. Lett.* **98**, 022002 (2007).
- [3] B. Aubert *et al.* (BABAR Collaboration), *Phys. Rev. D* **74**, 031102(R) (2006).
- [4] The charge-conjugate modes of all decays in this paper are implied unless explicitly stated otherwise.
- [5] B. H. Behrens *et al.*, (CLEO Collaboration), *Phys. Rev. Lett.* **80**, 3710 (1998).
- [6] B. Aubert *et al.* (BABAR Collaboration), *Phys. Rev. Lett.* **92**, 061801 (2004).
- [7] H. J. Lipkin, *Phys. Lett. B* **254**, 247 (1991).
- [8] M. Beneke and M. Neubert, *Nucl. Phys.* **B651**, 225 (2003).
- [9] S. Nishida *et al.* (Belle Collaboration), *Phys. Lett. B* **610**, 23 (2005).
- [10] D. Atwood *et al.*, *Phys. Rev. Lett.* **79**, 185 (1997).
- [11] A. Abashian *et al.* (Belle Collaboration), *Nucl. Instrum. Methods Phys. Res., Sect. A* **479**, 117 (2002).
- [12] S. Kurokawa and E. Kikutani, *Nucl. Instrum. Methods Phys. Res., Sect. A* **499**, 1 (2003), and other papers included in this volume.
- [13] P. Koppenburg *et al.*, (Belle Collaboration) *Phys. Rev. Lett.* **93**, 061803 (2004).
- [14] C. Amsler *et al.* (Particle Data Group), *Phys. Lett. B* **667**, 1 (2008).
- [15] Events are generated with the CLEO QQ generator (see <http://www.lns.cornell.edu/public/CLEO/soft/QQ>); or the EVTGEN generator: D. J. Lange, *Nucl. Instrum. Methods Phys. Res., Sect. A* **462**, 152 (2001); Detector response is simulated with GEANT: R. Brun *et al.*, GEANT 3.21, CERN Report No. DD/EE/84-1, 1984.
- [16] R. A. Fisher, *Annals of Eugenics* **7**, 179 (1936).
- [17] The Fox-Wolfram moments were introduced in G. C. Fox and S. Wolfram, *Phys. Rev. Lett.* **41**, 1581 (1978); The modified moments used in this analysis are described by S. H. Lee *et al.* (Belle Collaboration), *Phys. Rev. Lett.* **91**, 261801 (2003).
- [18] J. Dragic *et al.* (Belle Collaboration), *Phys. Rev. Lett.* **93**, 131802 (2004).
- [19] H. Kakuno *et al.* (Belle Collaboration), *Nucl. Instrum. Methods Phys. Res., Sect. A* **533**, 516 (2004).
- [20] T. Skwarnicki, Ph.D. thesis, Institute for Nuclear Physics, Krakow, 1986; DESY Internal Report No. DESY F31-86-02, 1986.
- [21] H. Albrecht *et al.* (ARGUS Collaboration), *Phys. Lett. B* **241**, 278 (1990).
- [22] K. Cranmer, *Comput. Phys. Commun.* **136**, 198 (2001).
- [23] M. Iwasaki *et al.* (Belle Collaboration), *Phys. Rev. D* **72**, 092005 (2005).
- [24] B. Aubert *et al.* (BABAR Collaboration), *Phys. Rev. Lett.* **93**, 081802 (2004).
- [25] K. Abe *et al.* (Belle Collaboration), *Phys. Lett. B* **511**, 151 (2001).
- [26] B. Aubert *et al.* (BABAR Collaboration), *Phys. Rev. D* **72**, 052004 (2005).
- [27] T. Sjostrand, *Comput. Phys. Commun.* **82**, 74 (1994).
- [28] A. L. Kagan and M. Neubert, *Eur. Phys. J. C* **7**, 5 (1999).